3D Solution of Hartree-Fock-Bogoliubov Equations for Drip-Line Nuclei

J. Terasaki, P.-H. Heenen*
Service de Physique Nucléaire Théorique,
U.L.B.-C.P.229, B-1050 Brussels, Belgium

H. Flocard
Division de Physique Théorique† Institut de Physique Nucléaire,
91406 Orsay Cedex, France

P. Bonche
SPhT ‡-CE Saclay, 91191 Gif sur Yvette Cedex, France

February 9, 2008

Abstract

We investigate the possibility of describing triaxial quadrupole deformations for nuclei close to the two-neutron drip line by the Hartree-Fock Bogoliubov method taking into account resonances in the continuum. We use a Skyrme interaction to describe the Hartee-Fock hamiltonian and a density-dependent zero-range interaction to evaluate the pairing field. The mean-field equations are solved in a three-dimensional cubic mesh. We study the stability of the two-neutron separation energies and of the description of the nuclear surface as a function of the number of active mean-field orbitals and of the size of the mesh. The even Ni isotopes are used as a test case and the accuracy as a function of quadrupole deformation is studied by performing constrained calculations. A first application to the study of the two-neutron separation energies in Ni isotopes up to the drip line is presented.

*Directeur de Recherches FNRS.
†Unité de recherches des Universités Paris XI et Paris VI associée au CNRS.
‡Laboratoire de la DSM

1 Introduction

Radioactive beam facilities, whether already active or soon to come, will enlarge our knowledge of the nuclear structure far away from the stability valley [1, 2]. They will allow a complete investigation of the drip lines for the light elements. Beyond their importance for models aiming at describing catastrophic astrophysical processes, such experiments give the possibility to address questions related to our understanding of single-particle or quasi-particle mean-field approximations. One of these questions concern the isospin properties of the nuclear interaction [3] which plays a major role in determining the location of the drip lines. Another one [4, 5] is related to the stability of the shell effects and of the magic numbers in the vicinity of the drip line. This stability depends in part on the modifications of the spatial structure of the single-particle potential and especially of its surface. Large values of $\mid N - Z \mid$ may also generate some decoupling between the proton and neutron mean-fields. In that respect, a still open question is the existence of nuclei with neutron and proton densities showing different deformations [6, 7].

Several extensive studies of exotic nuclei using macroscopic-microscopic methods are already available [8, 9, 10, 11]. They make predictions for binding energies, radii and deformations. However these methods assume a simple parametrization of the shape of the mean-field and of its radial dependence. Thus, it is difficult to take unambiguously into account effects related to a large excess of neutrons especially when they generate exotic phenomena such as halos or neutron skins[2]. Most studies run into difficulties because, in the vicinity of the drip line, the Strutinsky method requires that one takes into account resonant single particle states [12]. Microscopic methods such as Hartree-Fock (HF) or Hartree-Fock-Bogoliubov (HFB) which let

the mean-field adjust self-consistently to the dynamical conditions associated with a specific N, Z configuration are better suited for theses studies.

The calculation of nuclear properties in the vicinity of the drip lines is made difficult by the very precise phenomenon which defines them: the Fermi level of one nucleon species becomes close to zero. As the Fermi energy diminishes the active pairing space extends into the continuum, and achieving a correct description of pairing correlations becomes a major problem. Simple methods such as HF+BCS are no longer valid because they predict a leakage of nucleons into the continuum. The HFB method however provides a remedy to this deficiency as it allows the coupling to positive energy resonant states while preserving confinement of the nuclear density [13, 14]. As a consequence, one must achieve an accurate description of the resonances which are immersed in a sea of continuum states. This question has been successfully dealt with in studies restricted to spherical nuclei [15].

Static deformations near the neutron drip line have been observed for Sodium and Magnesium isotopes [16] and are inferred for some Sulfur elements from their β decay properties [17]. Studies of these nuclei have been limited to shell model calculations including two major shells [18, 19] and to pure HF or relativistic Hartree calculations [7]. All these methods are of limited applicability for heavy nuclei, either because the calculations become untractable or due to the absence of a correct treatment of pairing correlations. In this work we present a method which allows a solution of the HFB equations in three dimensions and opens therefore the possibility of an investigation of deformed neutron-rich nuclei. The above described problems are especially acute near the neutron drip line. Indeed, in the vicinity of the proton drip line, the existence of the coulomb barrier allows to circumvent them easily at least for a determination of global observables (energy, density distribution) although not for more detailed

properties such as the lifetime of proton emitters. For this reason, all the calculations presented in this work will concern the neutron-rich side of the nuclear chart.

Our method is similar to that developped to study rotating nuclei [20, 21]. The next section briefly recalls some characteristics of the method. It presents the modifications necessary for an investigation of neutron-rich nuclei and defines the parameter which control the numerical accuracy. In Sect. 3 we discuss the numerical tests which establish the quality of our method. Sect. 4 gives a first application to a series of Ni isotopes. The last section collects our conclusions.

2 The Method

We have developed a method to solve the HFB equations by discretization of a rectangular box [6]. This has the advantage over methods relying on expansion on a basis that nuclei with much different deformations can be treated at the same level of accuracy. In this section, we introduce our notations, paying special attention to the points which require some particular care in the treatment of nuclei far from stability.

Let us start by a brief reminder of the HFB equations for time-reversal invariant states. We write them as a function of basis states $i, \bar{i}$ related by a time reversal operation. The HFB equation is

$$\begin{pmatrix} h-\lambda & \Delta \\ \Delta^* & -h+\lambda \end{pmatrix} \begin{pmatrix} U \\ V \end{pmatrix} = \begin{pmatrix} U \\ V \end{pmatrix} E_l \ , \tag{1}$$

where λ is the chemical potential, h the mean-field hamiltonian:

$$h_{ij} = T_{ij} + \sum_{kl} (V_{ikjl} + V_{i\bar{k}j\bar{l}})\rho_{kl} \quad , \tag{2}$$

and Δ the pairing gap matrix**:**

$$\Delta_{ij} = \sum_{kl} V_{i\bar{j}\bar{k}l}\kappa_{\bar{k}l} \quad . \tag{3}$$

In these expressions, the one-body density matrix ρ and the pairing tensor κ are defined by:

$$\rho = \left(VV^{+}\right) \quad , \quad \kappa = \left(UV^{+}\right) \quad . \tag{4}$$

In order to simplify the numerical resolution of the HFB equation and to make easier an adjustment of the effective nucleon-nucleon force from which the matrix elements V are calculated, we decided to use two different forces, one acting in the particle-hole (ph) channel and the other in the particle-particle (pp) channel. The mean-field hamiltonian h is calculated according to eq. (2) with a Skyrme force, the numerical results presented below have been obtained with the parametrization SIII [22]. In the pp-channel, we evaluate the pairing gap matrix Δ (3) by means of a zero-range density-dependent pairing force [21]:

$$V_{\rm P}(\mathbf{r}_1, \mathbf{r}_2) = V_0 \left(1 - P_\sigma\right) \left(1 - \frac{\rho(\mathbf{r}_1)}{\rho_{\rm c}}\right) \delta(\mathbf{r}_1 - \mathbf{r}_2) \quad . \tag{5}$$

In the definition of $V_{\rm P}$, P_σ is the spin exchange operator and $\rho(\mathbf{r})$ the total density in coordinate space. The pairing strength is controlled by V_0 while $\rho_{\rm c}$ determines the $\mathbf{r}$-dependence of the pairing gap field.

In a previous study [21], we have observed that a pairing field acting over the entire volume of the nucleus yields a poorer reproduction of moments of inertia than a surface peaked pairing field. Since surface properties may play also a strong role for neutron rich nuclei, we choose a surface-peaked pairing field. Within the parametrization (5) this is achieved by selecting a value of ρ_c close to the nuclear saturation density. As this paper is devoted to the analysis of the convergence properties of our method, we have differed an investigation of the influence of the values of V_0 and $\rho_{\rm c}$ on the properties of nuclei far from stability.For this reason, we have chosen to use the values given in ref [12] ($V_0 = 1128.75 MeV\ fm^3$ and $\rho_{\rm c} = 0.13354 fm^{-3}$). In fact, we have also checked that the numerical properties of our method are not affected by an

increase of 20% of these values. Finally our pairing force is determined by a third parameter: an energy-cutoff Λ which controls the energy width of the pairing active space. In this work, this space extends up to 5 MeV above the Fermi surface. Since we are concerned with nuclei whose neutron chemical potential λ is negative but close to zero, our HFB calculation takes therefore into account resonances up to 5 MeV in the continuum. Technically speaking, one must introduce Λ to guarantee the existence of a solution to the HFB equations with a zero range pairing force such as $V_{\rm P}$. The cutoff can be interpreted as a crude way of simulating the introduction of a finite range which is known to ensure the convergence of the HFB equations. In order to select the magnitude of Λ, it is useful to remember the physical motivation behind the HFB formalism. It aims at describing the action of pairing correlations *in the vicinity* of the Fermi surface. The energy scale typical of those correlations is given by the magnitude of the pairing gap. For nuclei, it is experimentally known to be of the order of 1 MeV. We therefore think that the value of Λ adopted in this work (5 MeV) is sufficiently large to preserve the physically important features of the HFB approximation while eliminating the divergence resulting from the high relative momentum behavior of the matrix elements of a zero-range force. Our choice for the cutoff eliminates a possible coupling of HFB eigenstates associated with deep hole states to the eigenstates of the continuum. As discussed in ref. [13, 23], such a coupling generates a width for deep hole states. As a matter of fact, this phenomenon is by no means specific of nuclei far from stability, however it is generally neglected. Besides, the physical interpretation of such widths, as well as their observation, is presumably very difficult, especially if they turn out to be smaller than those resulting from other broadening mechanisms [24].

Because the wave-functions of time reversed orbitals are related to each other in a simple

way, we only have to consider the member i of each pair $(i, \bar{\imath})$. From now on, when we will mention a number of orbitals, that will be the number of i-orbitals. Moreover, because in the 3D calculations presented below we impose three planes of symmetries for the nuclear density, we only have to store the values of the single-particle wave-functions in one spatial octant.

The HFB equation are solved in coordinate space by means of the two-basis method described in ref. [20]. The coordinate space technique allows to work with a limited number of basis states however large enough to ensure a good level of accuracy. In particular our method describes equally well the interior and the surface of the nucleus as long as the calculations are performed in a box sufficiently large to enclose the nucleus and the tails of both the density and the pairing tensor. This point will be discussed below. The method of solution relies on two nested loops of iterations. In the outer one, the eigenstates of h are determined by the imaginary time-step method [25]. In the inner loop the HFB equations are solved, which gives U, V, ρ and κ according to eqs. (1-4). It is also in this loop that the value of λ is determined by a constraint on the particle number.

We denote by $\phi_i(\mathbf{r}, \sigma)$ the single-particle component of spin σ of the i$^{\text{th}}$eigenstate of h and e_i its eigenvalue. On this basis, refered to as the HF basis, the pairing operator Δ_{ij} is given by:

$$\Delta_{ij} = \int d\mathbf{r} \Psi^*_{ij}(\mathbf{r}) \widetilde{\Delta}(\mathbf{r}) \ , \tag{6}$$

where

$$\Psi_{ij}(\mathbf{r}) = \sum_{\sigma} \phi_i(\mathbf{r}, \sigma) \phi_j(\mathbf{r}, \sigma)^* \quad , \quad \widetilde{\Delta}(\mathbf{r}) = V_0 (1 - \frac{\rho(\mathbf{r})}{\rho_{\text{c}}}) \sum_{kl} \Psi_{kl}(\mathbf{r}) \kappa_{kl} \quad . \tag{7}$$

The function $\widetilde{\Delta}(\mathbf{r})$ is the local pairing gap in the coordinate representation.

The second basis, usually called the canonical basis, is built from the eigenvectors φ_i of the

density matrix ρ:

$$(W^\dagger \rho W)_{ij} = n_i \delta_{ij} \quad , \quad \varphi_i = \sum_j W^t_{ij} \phi_j \quad . \tag{8}$$

The eigenvalues n_i are interpreted as occupation probabilities. In particular, the local density in coordinate space is given by

$$\rho(\mathbf{r}) = \sum_{i\,\sigma} n_i |\varphi_i(\mathbf{r}, \sigma)|^2 \ , \tag{9}$$

The feedback of the internal loop on to the external one is achieved via the dependence of h on $\rho(\mathbf{r})$ and on other densities. A characteristic of our numerical method is the imaginary time-step algorithm, which enables us to carry *only* the eigenstates of h for the physics that we want to study, even though the dimension of the basis states associated with our spatial discretization inside a cubix box is of the order of several ten thousands. In the next section, we especially study the convergence properties of the numerical algorithm with respect to the number of eigenvectors in the HF **or** canonical basis followed with the imaginary time-step method.

3 Numerical Analysis of the Discretization of HFB equation

Before studying a chain of isotopes, we discuss the influence of the continuum on the HFB solution for the neutron rich nucleus ^{84}Ni. To solve the HFB equations, we impose that the density vanishes at the edges of the box, the resulting boundary conditions imply that the positive energy spectrum is discretized. Thus we have to investigate the convergence of the results with respect to the size of the box.

Our choice of ^{84}Ni is motivated by two reasons. First this nucleus has a large neutron excess with a neutron Fermi energy close to zero (-0.98 MeV). Second, $Z = 28$ is a well defined magic

number and proton pairing correlations vanish. This simplifies our analysis as it allows a study of protons within the Hartree-Fock approximation, limiting thereby our HFB study to effects of the continuum on neutron pairing only. Furthermore, again because of the proton magicity, the ground state is spherical. We can therefore solve the problem in a cube and investigate the convergence versus the only remaining numerical parameter of the problem: namely the dimension R of the cubic box. Let us recall however that in our method of solution of the mean-field equations, spherical configurations are treated in the same way as axial and triaxial deformed ones.

3.1 Single-Particle Spectrum

According to the presentation of the two-basis method, two different sets of orbitals are considered in HFB calculations: the HF-basis (eigenstates of h with eigenvalues e_i) and the canonical basis (eigenstates of ρ with eigenvalues n_i). These two sets, identical in the BCS limit, are not very different. Since their global features are similar, we discuss first the canonical basis. We will later point out some of their differences in the particuliar case of resonant states.

In Figure 1, we have plotted the diagonal elements h_{ii} of the mean-field hamiltonian in the canonical basis as a function of the box size for the states in the vicinity and above the Fermi level. As expected, two different classes appear in the positive energy part of the diagram. First some are stable with respect to R, they correspond to resonances. For the others, that we will refer to as continuum states, h_{ii} is a steadily decreasing function of R. Each resonance possesses quantum numbers which allow an unambiguous assignment to a single-particle shell model state. In one case ($1h11/2$), the resonant states are crossed by continuum states as R grows. Note that due to the fact that spherical symmetry is not imposed in our calculation,

the degeneracy between the different subshells is slightly removed.

Figure 2 shows that the occupation n_i of the resonant states is small but non negligible. It is also stable versus R. Nevertheless, one observes a slight decrease of n_i. This phenomenon can be correlated to the evolution of h_{ii} for the $3s_{1/2}$ bound state whose energy decreases slowly as a function of R (see figure 1). Within the HFB formalism, this could reflect a coupling of this bound state to the continuum. On the other hand, since the effect is observed for an s-state, it may also be due to the improved description of the nuclear potential at large distance as the box size increases. In order to test the latter hypothesis, we have performed HF calculations in boxes of growing sizes. In this case, we have found that the energy of the $3s_{1/2}$ particle state decreases by 400 keV as the box size varies from 11 to 15 fm. Therefore we can assert that improving the description of the nuclear surface is the main cause for the lowering of the $3s_{1/2}$ energy. In fact, pairing correlations acts only as a second order effect by slightly reducing the lowering. Within the HFB formalism, this lowering of the $3s_{1/2}$ energy translates into an increase of occupation probability which can be observed in the upper part of figure 2. As a consequence, because all occupations add up to the neutron number N, the n_i's of the resonances diminish. Figure 2 shows also that the occupation of all the continuum states remain zero, irrespective of the value of h_{ii}. In particular, for the largest box sizes, some of these states are below resonant states with non zero occupation.

The main difference between the HF and canonical bases is that resonant orbitals can be unambiguously identified only in the latter one. The mixing of resonant and continuum states in the HF basis has many consequences. First, the evolution versus R of the diagonal matrix elements of ρ in the HF basis is not as simple as the one shown on figure 2. Accidents occur for values of R such that a continuum state crosses a resonance. A study of the wave-functions for

the resonant and continuum states also shows this qualitative differences between both bases. Let us consider for instance the six resonant eigenstates of ρ for which h_{ii} is constant and close to 3.1 MeV when R varies from 11 to 15 fm, grouped under the symbol [on figure 1. These eigenstates can be assigned to the spherical $1h_{11/2}$ level. In the canonical basis, their wave-functions φ_i are localized near the origin. In that respect, they differ significantly from continuum states with similar values of h_{ii}. On the other hand, in the HF basis, when R is between 13 to 15 fm, there are *eight* states with e_i close to 3 MeV with wave-functions ϕ_i having a large amplitude near the origin. These wave-functions exhibit also a tail at large distances, which indicates that the decoupling between resonant states and continuum is not realized in the HF basis. As an example, we show in the lower part of figure 3 the quantity $\sum_\sigma |\varphi_i(x, y, 0, \sigma)|^2$ for one of the $1h_{11/2}$ states. In contrast, the upper part shows $\sum_\sigma |\phi_i(x, y, 0, \sigma)|^2$ for the HF-orbital having the maximum overlap with this resonance. The latter function displays a tail beyond 9 fm that is not present for the corresponding quantity in the canonical basis. This comparaison confirms that the canonical basis is the relevant one for the analysis of the resonances.

3.2 Total Energy and Two-Neutron Separation Energy

We turn now to global observables to study the stability of our results as a function of the number of states available for the description of the continuum. Figure 4 shows the total energy of ^{84}Ni as a function of R. When the number of HF (or canonical) basis states is at least equal to 60, convergence is achieved. The R-converged value of the energy is determined with an accuracy better than 100 keV when the box size is equal to 12 fm. The behavior of the curve obtained with 55 neutron states can be understood from figure 1. For R greater than 14 fm, the $1h_{11/2}$ resonance has been crossed by some continuum states. With 55 states

only, one cannot account simultaneously for these continuum states and the 6 states of the resonance. The increase of E reflects therefore the loss of pairing energy due to some resonant states leaving the active pairing space.

As can be seen from figure 4, the larger the box, the more states one needs to reproduce correctly the total energy, up to 80 states at least in a 17 fm box. Indeed, as the size of the box increases, one need more and more states to describe correctly both the resonances and the continuum to which they couple. This is confirmed by figure 5 which gives the two-neutron separation energies $S_{2n}(N,Z) = -E(N,Z) + E(N-2,Z)$. Already for R=12 fm, this quantity, which determines the location of the drip line, can be calculated with a precision better than 100keV, when the basis includes at least 60 states.

Finally, one must mention that the convergence of E versus R is better than that achieved for its separate components (kinetic, potential, spin-orbit, pairing), which is a usual feature of a variational method such as HFB. For instance, the variation of the pairing energy when R increases from 11 fm to 15 fm is of the order of 0.5 MeV when 70 basis states are used.

3.3 Density and Pairing Field

Since the possible existence of halos or neutron skins motivates in part our interest in neutron-rich nuclei, it is important to determine how well we can calculate the tail of the nuclear density. In figure 6 using a logarithmic scale, we have plotted the neutron density of ^{84}Ni for several box sizes. For R larger than 14 fm, the density can be predicted with good accuracy over 4 decades (i.e. up to 13 fm). The comparison between the neutron and proton densities does show the existence of a neutron skin in this neutron rich nucleus.

In figure 7, we compare the radial distribution of the neutron pairing field $\widetilde{\Delta}_n$ (7) with the

neutron and total densities. The pairing field extends further than the density by about 2 fermi. This point has been discussed in ref. [14] where it was shown that, due to contributions of HFB eigenstates with quasi-particle energy larger than $|\lambda|$, the density decreases asymptotically faster than the pairing tensor. From a practical point of view, it means that the box size must be large enough to accomodate the spatial extension of $\widetilde{\Delta}_{\rm n}$. This indicates that there must be an adequation between the cut-off in coordinate space introduced by the box and the parameters of the pairing interaction.

Let us discuss the problems associated with the 3 parameters of the pairing interaction (equ. 5). We have checked that an increase by 20% of the value of the pairing strength V_0 does not modify the quality of convergence with respect to R. The critical density ρ_c that we have used here is smaller than in [21], leading to a more surface peaked pairing field. This value therefore amplifies the surface character of the pairing field and the conclusions of the present work should not be affected by an adjustment of this density factor. The third parameter of the pairing interaction is its cut-off. To check a consequence of the change of this cut-off, we have performed calculations without any. This is equivalent to introduce an implicit R dependant cutoff $\Lambda(R)$ determined by the number of basis states. From figure 1 one sees that for 70 basis states, $\Lambda(R)$ decreases from a value larger than 10 MeV for $R = 11$ fm to about 6 MeV for $R = 15$ fm. With such a number of orbitals, the sensitivity versus the box dimension is enhanced: the total energy E varies by 0.3 MeV when R increases from 12 to 15 fm. This indicates that the larger the cut-off (i.e. the greater Λ), the larger the required number of orbitals.

3.4 Deformation Energy Curve

One of the questions we want to address in the future is the influence of static deformations on the position of the drip line. Because they are proton magic, Ni isotopes are spherical. To test the ability of our model to describe deformed nuclei, we have enforced deformations by means of a constraint on the quadrupole moment for ^{92}Ni. We have chosen this nucleus, instead of ^{84}Ni, as it is in our calculation the last stable Ni isotopes against two-neutron emission before the drip line (see next section). Figure 8 presents thus the axial deformation energy curve of ^{92}Ni as a function of the mass quadrupole moment. In figure 9, we show that prolate and oblate excitation energies at fixed quadrupole moments are stable versus the box size. This demonstrates that we can calculate spherical and deformed HFB solutions of neutron-rich nuclei with similar accuracy.

For a dimension of the basis equal to 70, we find that the convergence with respect to R of the absolute energies is not as good as it was for ^{84}Ni: when R grows from 12 to 15 fm, we observe a variation of 0.1 MeV. Increasing the basis size to 80 mean-field wave-functions brings a gain of energy of 50 to 100 keV for each box size and decreases the amplitude of the variation with R to 50 keV. This enables us to estimate the errors on total energies to be of the order of 100 to 200 keV with 70 wave-functions for ^{92}Ni, which is still sufficient for an accurate description of two-neutron separation energies.

The results discussed in the last section have been obtained with a box size equal to 15 fm and 70 basis states. A smaller box is definitively not appropriate whereas a larger one demands more states without any significant improvement of the results.

4 Ni Isotopes two-neutron Separation Energies

As a first application of our method, we have considered the Ni isotopic chain, which is experimentally known up to ^{78}Ni [26]. The two-neutron separation energies S_{2n} are shown in figure 10. The comparison with experiment [27] is satisfactory. The two major accidents in the curve correspond to the magic numbers $N = 28$ and 50. The curve crosses zero at $A = 94$ which is therefore our prediction for the drip line associated with the emission of a neutron pair. In figure 10, we have also reported HFB spherical results of ref. [15] which have been calculated with the SkP interaction [14]. The overall slope is similar and the predictions for the position of drip line is the same. The SkP curve displays only very small slope changes at major shell crossings. This may be a consequence of the larger single-particle level density for the SkP force than for the SIII force. These different level densities are related to the differences between the effective mass values of SkP and SIII (1.0 and 0.75 repectively). The smooth behavior of the SkP curve may also be due to stronger pairing correlations. This will have to be checked by more extensive studies. On figure 10 the separation energy calculated from the position of the Fermi level (i.e. $-2.0 * \lambda_n$) is also plotted. It agrees nicely with the calculated S_{2n}, except around the magic neutron number N=50.

Let us finally mention that we have investigated the stability of our predictions for S_{2n} against the mesh size Δx of our calculation. Decreasing Δx from 1 fm to 0.75 fm results in a lowering of the S_{2n} by less than 50 keV over the entire series of isotopes. Such a small inacurracy does not modify our conclusions concerning the position of the drip line.

5 Conclusion

In this work, we have presented a method of solution of the HFB equation applicable to even nuclei in the vicinity of the drip lines. It is well suited to the study of the neutron drip line where continuum effects can become important especially when the description of pairing correlations is crucial. Our method is based on a discretization of the continuum in coordinate space and is naturally adapted to the investigation of nuclei either spherical or with a static quadrupole deformation. We have studied the convergence of physically relevant quantities (such as single-particle spectrum, binding energies and two-neutron separation energies, neutron density distribution) with respect to the dimension of the box in which calculations are performed. We have shown that for a large but still tractable number of basis states, we control this convergence, at least when the active range of the pairing interaction does not extends further than 5 MeV into the continuum. We have also shown how the size of the box is correlated with the number of basis states and how to choose these two quantities to achieve a reasonable convergence.

The method establishes a clean separation between positive energy resonant states which contribute to pairing and continuum states which are mere spectators of the dynamics. Our analysis has confirmed that the canonical basis is the most convenient to extract resonances out from the continuum. We have also checked the expected behaviours of the density and of the pairing gap field. In particular we have verified that the latter quantity extends further out than the density. A motivation of the present work is to devise a method suitable to investigate quadrupole deformation near the drip line. Therefore we have tested that the accuracy of our method does not depend on the deformation. This has been done by an analysis of an energy

curve obtained by means of a constraint on the quadrupole moment. However, the present analysis does not permit to investigate bound state widths resulting from a coupling to the continuum.

As a first application we have calculated the two-neutron separation energies for a series of Ni isotopes extending up to the neutron drip line. Our results agree with data when available [27]. We predict that the shell effect at $N = 50$ remains strong and that the drip line occurs at $N = 66$, namely for ^{92}Ni. This is in agreement with the former prediction of ref [15] using the SkP interaction.

Are all nuclei along the drip line spherical? We believe that we have in our hands the tool required to answer this question. An analysis of the predictions of recent effective interactions for quantities relevant for the astrophysical r-process is another of the tasks that we are now in position to carry out.

Acknowledgements

We thank J. Dobaczewski and W. Nazarewicz for interesting discussions. This work was supported in part by the contract PAI-P3-043 and by the ARC convention 93/98-166 of the Belgian Office for Scientific Policy.

References

[1] C. Detraz and D. C. Vieira, Ann. Rev. Nucl. Part. Sci. **39** (1989) 407

[2] A. Mueller and B. Sherril, Ann. Rev. Nucl. Part. Sci. **43** (1993) 529

[3] E. Chabanat, P. Bonche, P. Haensel, J. Meyer and R. Shaeffer, Phys. Scr. **T56** (1995) 31

[4] M. Beiner, R. J. Lombard and D. Mas, Nucl. Phys. **A249** (1975) 1

[5] J. Dobaczewski, I. Hamamoto, W. Nazarewicz and J. A. Sheikh, Phys. Rev. Lett. **72** (1994) 981

[6] P. Bonche, H. Flocard, P.-H. Heenen, S.J. Krieger and M.S. Weiss Nucl. Phys. **A443** (1985) 39

[7] T.R. Werner,J. A. Sheikh, W. Nazarewicz, M.R. Strayer, A.S. Umar and M. Misu, Phys. Lett. **B33** (1994) 303

[8] P. Möller and J. R. Nix, Atom. Data and Nucl. Data Tables, **39** (1988) 213

[9] P. Möller, J. R. Nix, W. D. Myers and W. J. Swiatecki, Atom. Data and Nucl. Data Tables, **59** (1995) 185

[10] Y. Aboussir, J. M. Pearson and A. K. Dutta, Nucl. Phys. **A549**(1992)155.

[11] F. Buchinger, J.E. Crawford, A. K. Dutta, J. M. Pearson and F. Tondeur, Phys. Rev. **C49** (1994) 1402

[12] W. Nazarewicz, T. R. Werner and J. Dobaczewski, Phys. Rev. **C50** (1994) 2860

[13] A. Bulgac, unpublished (1980)

[14] J. Dobaczewski, H. Flocard and J. Treiner, Nucl. Phys. **A422** (1984) 103

[15] J. Dobaczewski, W. Nazarewicz and T. R. Werner, Zeit. Phys. A in press

[16] C. Detraz et al. Phys. Rev. **C19** (1979) 164

[17] O. Sorlin et al., Phys. Rev. **C47** (1993) 2941

[18] A. Poves and J. Retamosa Phys. Lett. **B184** (1987) 311

[19] W. Warburton, J.A. Becker and B.A. Brown, Phys. Rev. **C41** (1990) 1147

[20] B. Gall, P. Bonche, J. Dobaczewski, H. Flocard and P.-H. Heenen, Z. Phys. **A348** (1994) 183

[21] J. Terasaki, P.-H. Heenen, P. Bonche, J. Dobaczewski and H. Flocard, Nucl. Phys. **A593** (1995) 1

[22] M. Beiner, H. Flocard, N. V. Giai and P. Quentin, Nucl. Phys. **A238** (1975) 29

[23] S. T. Belyaev, A. V. Smirnov, S. V. Tolokonnikov and S. A. Fayans, Sov. J. Nucl. Phys. **45** (1987) 783

[24] G. F. Bertsch, P. F. Bortignon, and R. A. Broglia, Rev. Mod. Phys. **55** (1983) 287

[25] K. T. R. Davies, H. Flocard, S. Krieger and M. S. Weiss, Nucl. Phys. **A342** (1980) 111

[26] Ch. Engelmann et al, Z. Phys. **A352** (1995) 351.

[27] A. H. Wapstra and G. Audi, Nucl. Phys. **A432** (1985) 55

Figure Captions

Fig. 1 Diagonal matrix elements of the HF Hamiltonian in the neutron canonical basis for ^{84}Ni. The calculatation is performed with 70 neutron single-particle wave functions as a function of the box size R. Solid and dashed curves denote positive and negative parity levels, respectively. The numbers of quasi degenerate levels corresponding to each resonance are indicated in paranthesis.

Fig. 2 Eigenvalues of the density matrix corresponding to the positive energy states and to the $3s_{1/2}$ bound state.

Fig. 3 Density probability of one of the $1h_{11/2}$ neutron wave functions calculated with R=15 fm in the HF (a) and canonical (b) basis.

Fig. 4 Total energy E of ^{84}Ni as a function of R obtained with a number of neutron wave functions varying from 55 to 80. The origin of the energies is arbitrary.

Fig. 5 Two-neutron separation energies S_{2n} for ^{84}Ni as a function of R and of the number of neutron wave-functions.

Fig. 6 Proton (dot-dashed-dashed) and neutron densities along a radius r. The dashe, solid and dot-dashed curves correspond to a calculation including 70 neutron wave-functions and R = 13, 15 and 17 fm, respectively. The dotted curve corresponds to R_{box} = 17 fm and 80 neutron wave functions.

Fig. 7 a) Neutron pairing gap $\widetilde{\Delta}_n(x)$ (see eq. (8)) for ^{84}Ni (R = 15 fm and 70 neutron wave functions) as a function of the radius (spherical configuration). b) Neutron (solid) and total (dashed) densities as a function of r.

Fig. 8 Potential energy curve of ^{92}Ni as a function of the axial quadrupole moment q (R = 15 fm and 70 neutron wave functions).

Fig. 9 Total energies E of ^{92}Ni as a function of R for prolate (open circles, q=3 b) and oblate (triangles, q=-4 b) configurations excited by approximately 1 MeV. The spherical configuration is taken as the zero for each value of R.

Fig. 10 Two-neutron separation energies S_{2n} of even Ni isotopes as a function of the mass number A: experimental data [27] (open circles), present work (solid circles) and results of ref. [15] (open triangles). The separation energies calculated from the position of the neutron Fermi level are also shown (crosses).

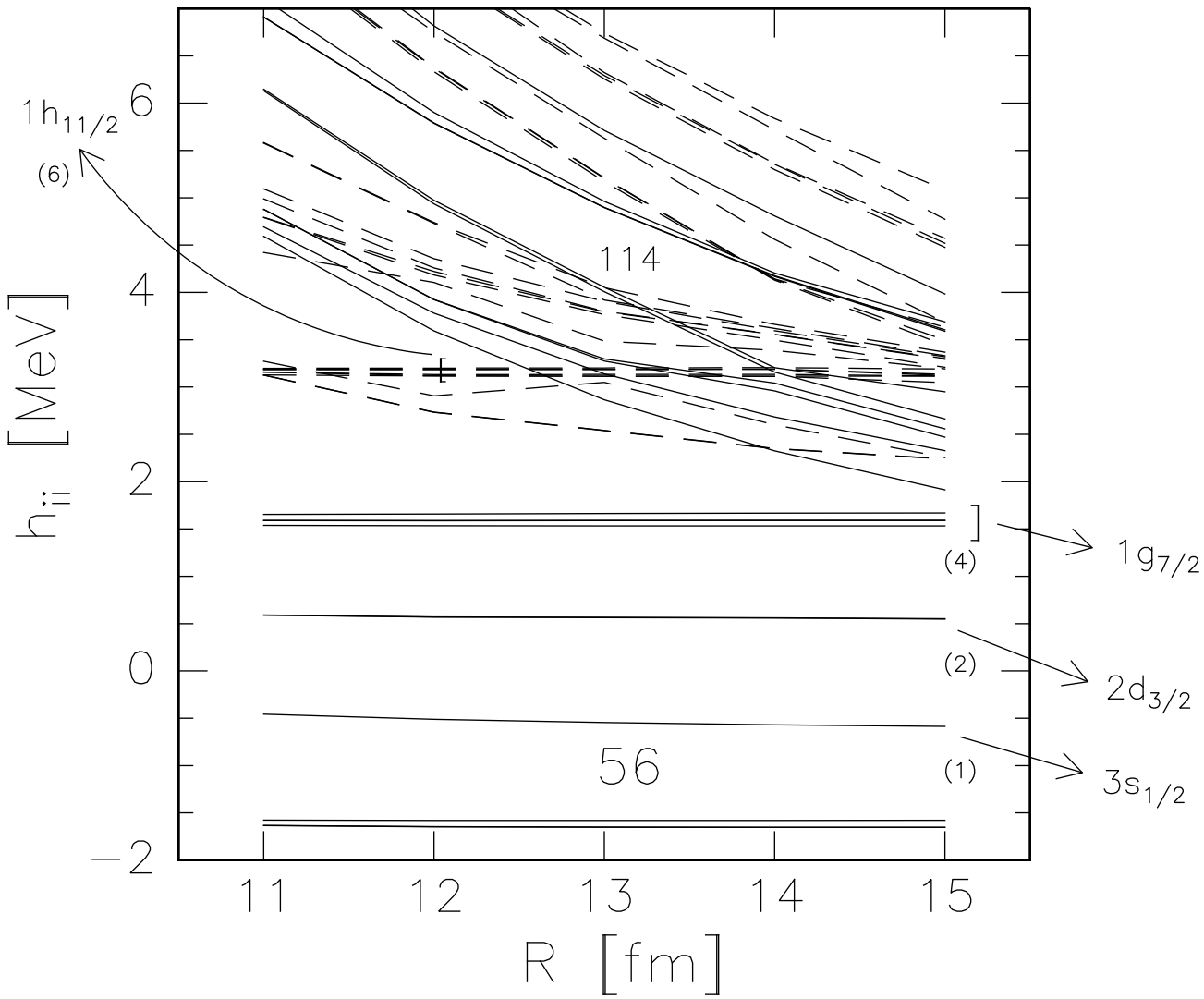
1h11/2
(6)
6
4
2
0
−2
hii [MeV]
114
56
]
(4)
1g7/2
(2)
2d3/2
(1)
3s1/2
11
12
13
14
15
R [fm]

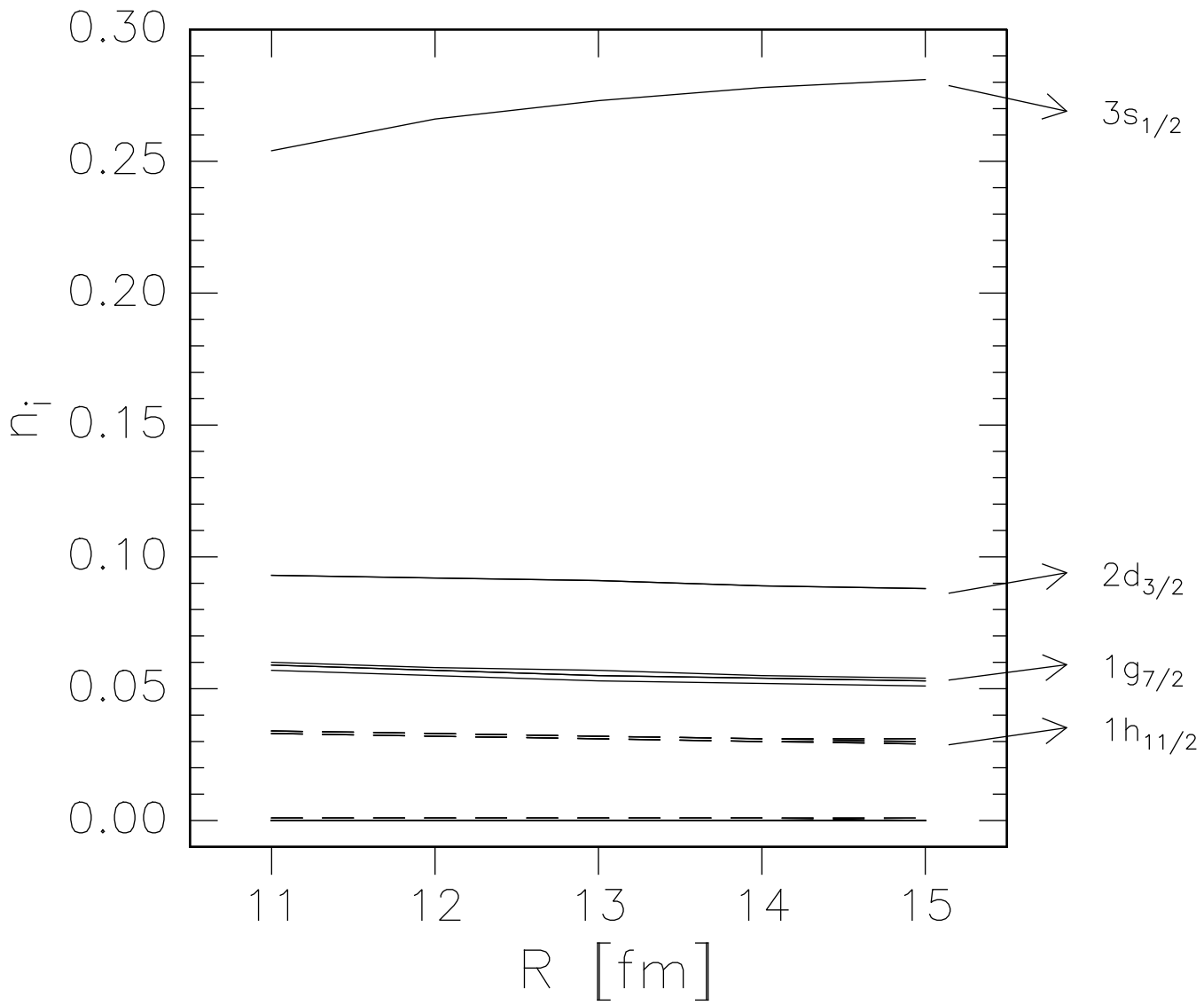
0.30
0.25
0.20
0.15
0.10
0.05
0.00
κ_i
11
12
13
14
15
R [fm]
$3s_{1/2}$
$2d_{3/2}$
$1g_{7/2}$
$1h_{11/2}$

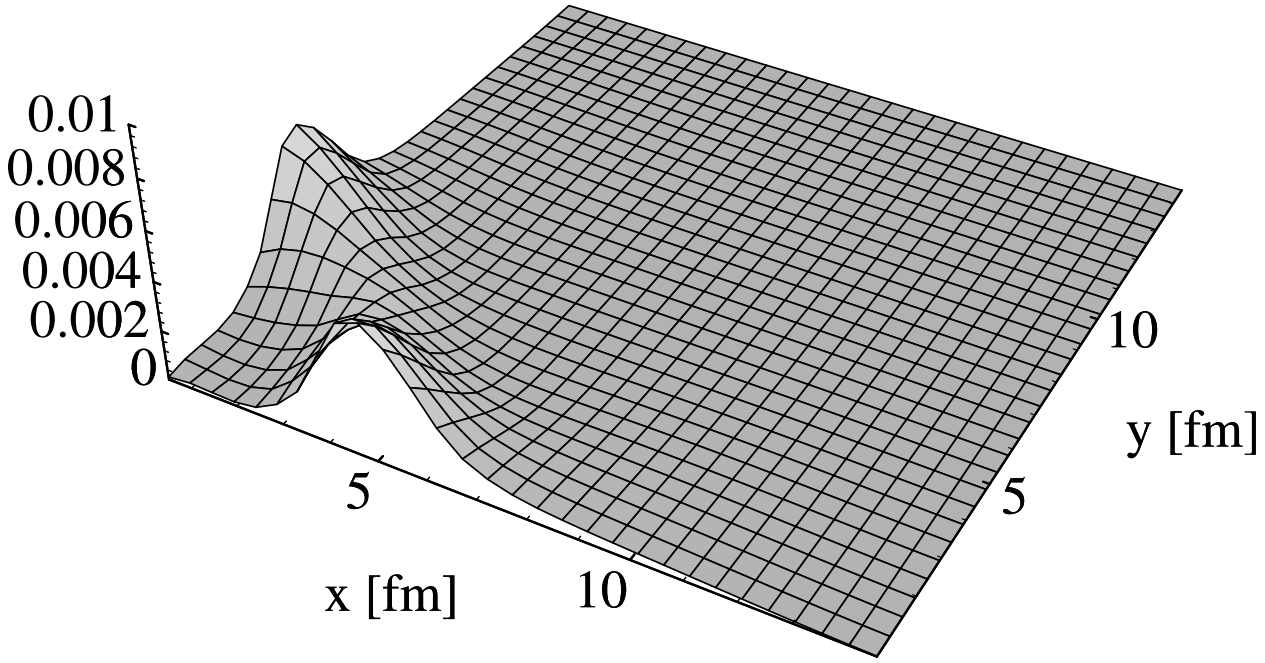
0.01
0.008
0.006
0.004
0.002
0
5
10
x [fm]
5
10
y [fm]

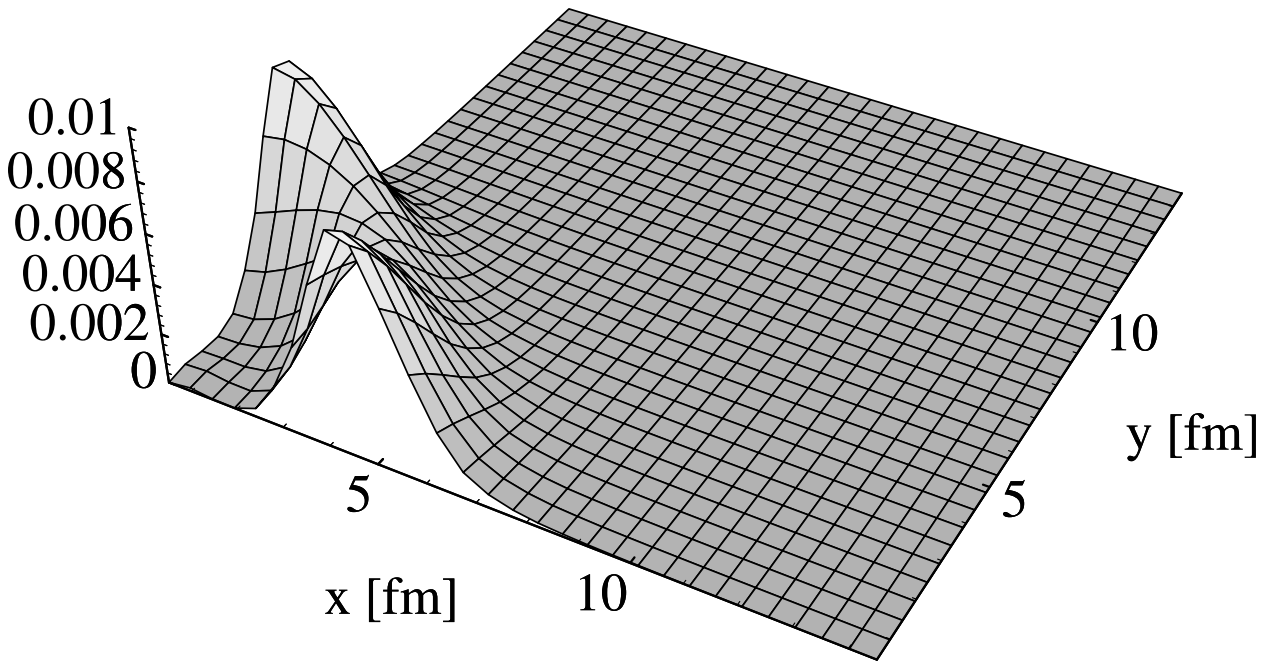
0.01
0.008
0.006
0.004
0.002
0
5
10
x [fm]
5
10
y [fm]

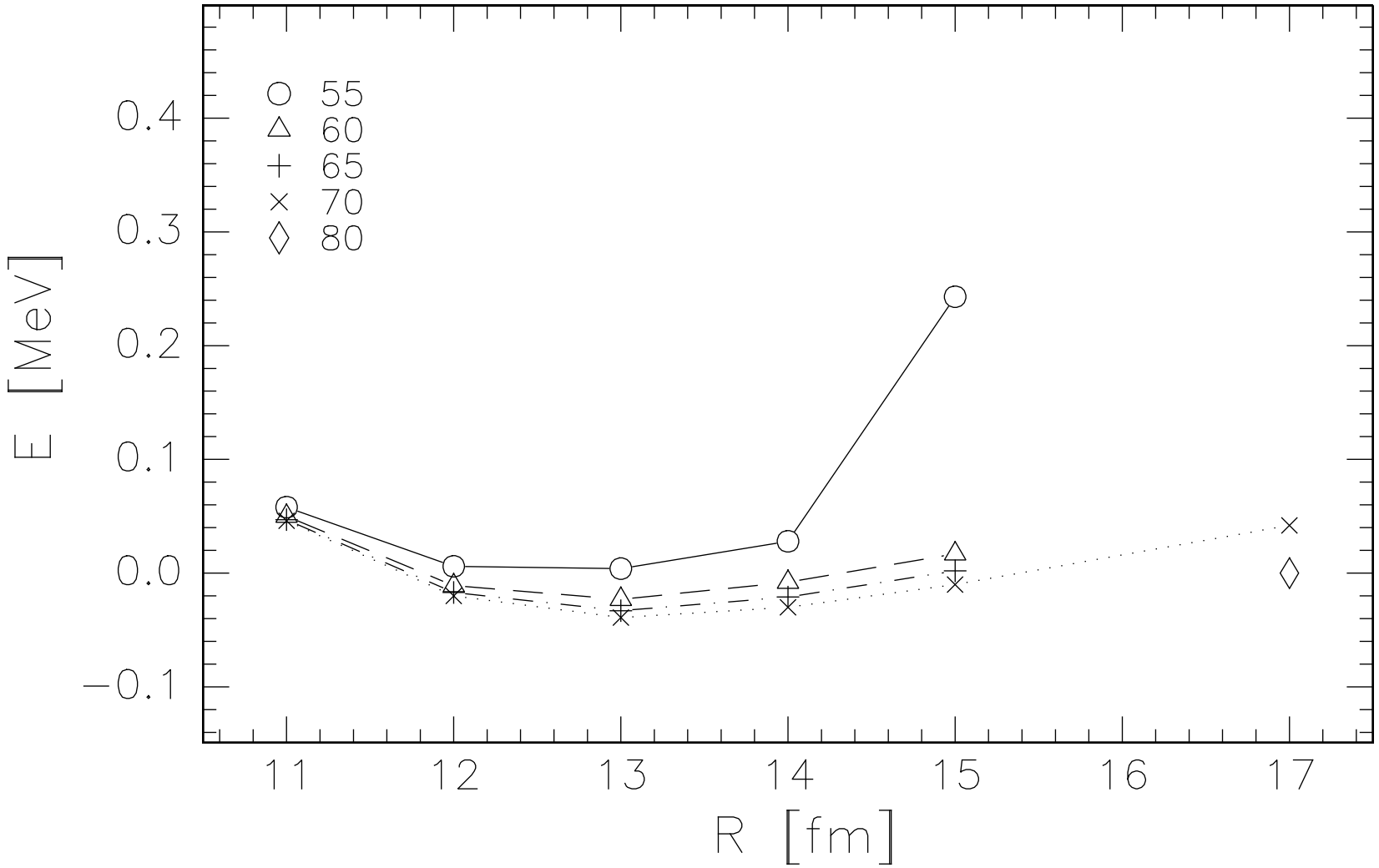
55
60
65
70
80
0.4
0.3
0.2
0.1
0.0
−0.1
E [MeV]
11
12
13
14
15
16
17
R [fm]

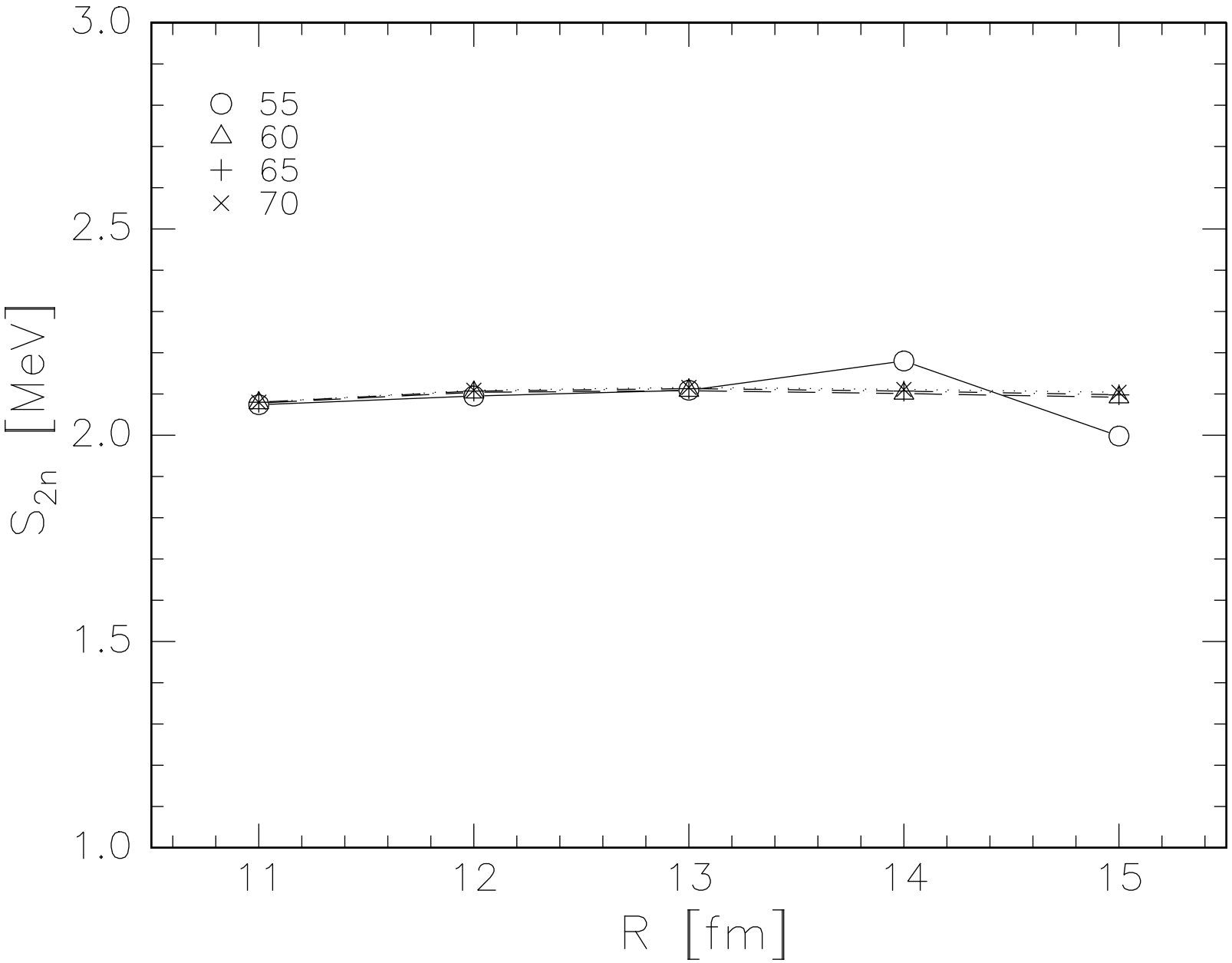
3.0
2.5
2.0
1.5
1.0
11
12
13
14
15
R [fm]
S_{2n} [MeV]
55
60
65
70

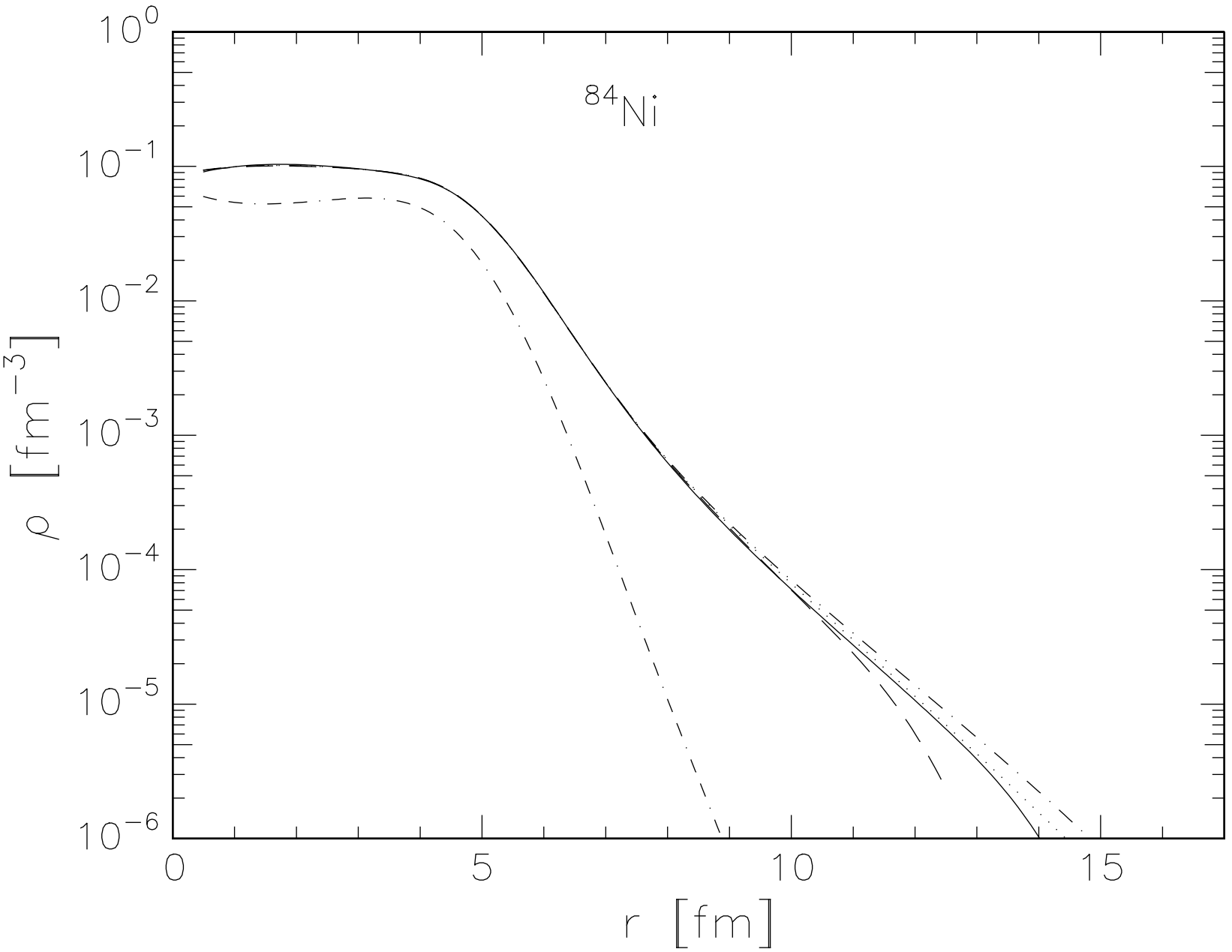
^{84}Ni
10^0
10^{-1}
10^{-2}
10^{-3}
10^{-4}
10^{-5}
10^{-6}
ρ [fm^{-3}]
0
5
10
15
r [fm]

r [fm]
0
5
10
15
ρ [fm⁻³]
0.00
0.05
0.10
0.15
0.20
b
ρn
ρtotal
Δn [MeV]
2
1
0
−1
−2
−3
a

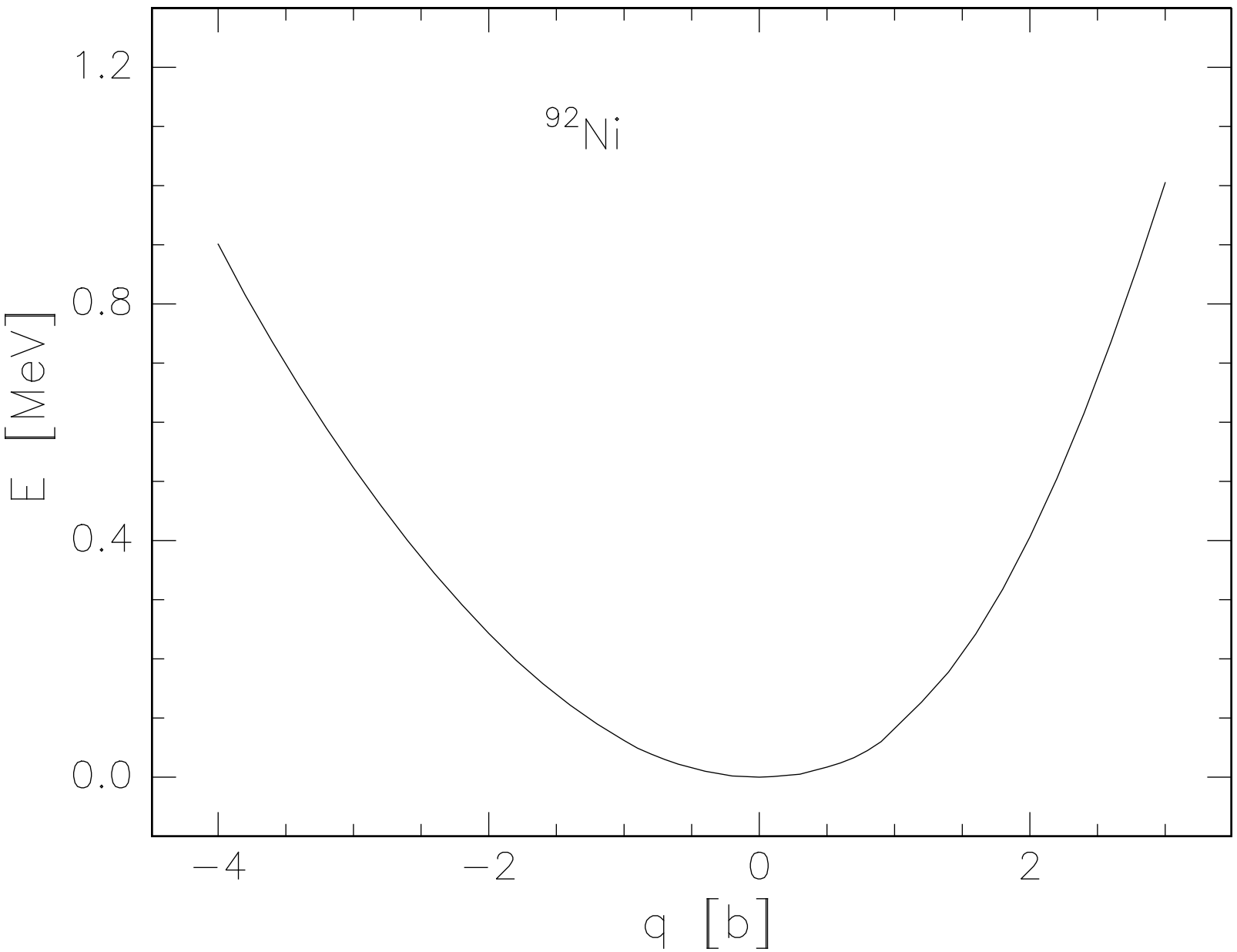
^{92}Ni
E [MeV]
1.2
0.8
0.4
0.0
−4
−2
0
2
q [b]

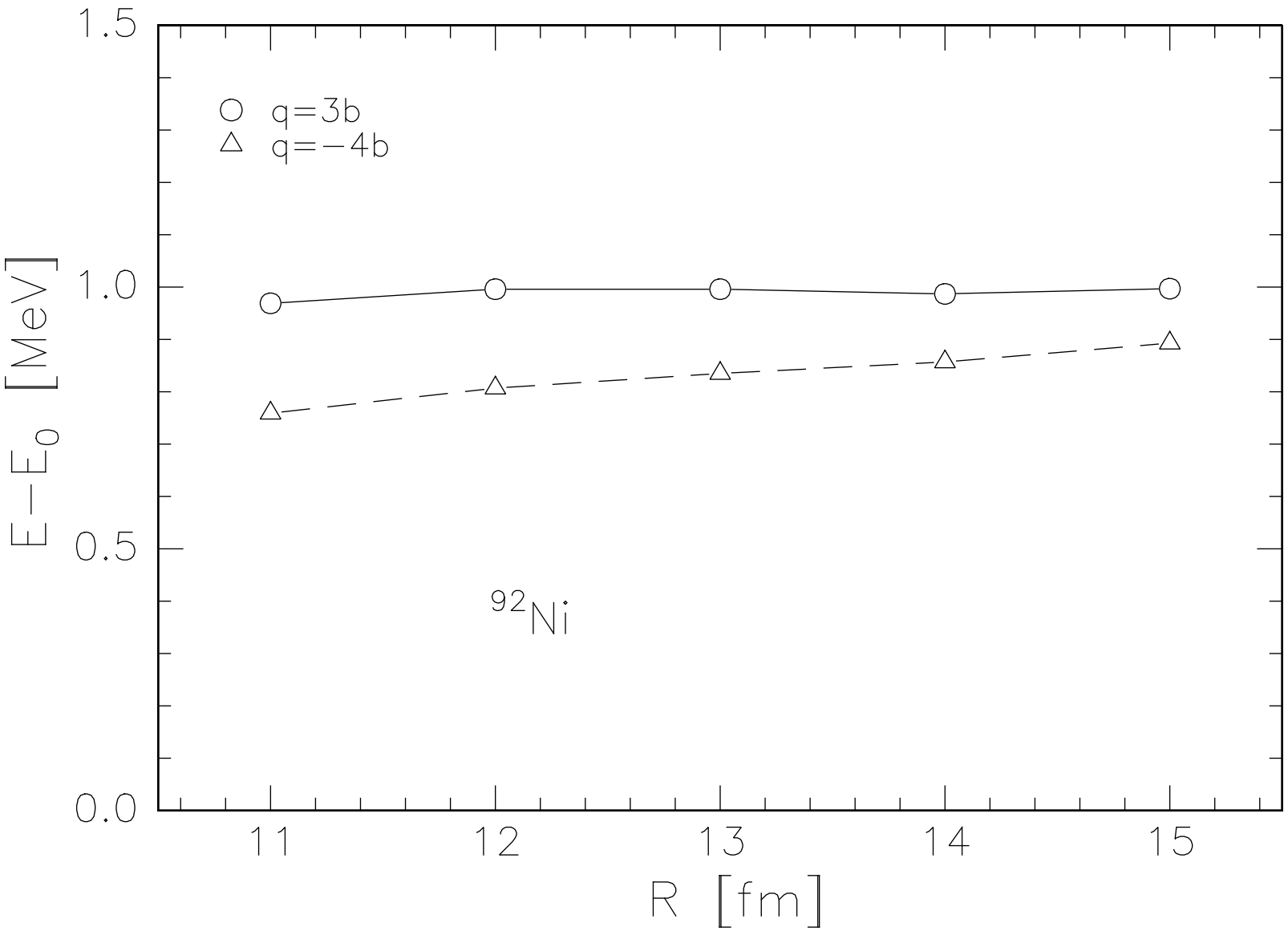
1.5
1.0
0.5
0.0
E − E0 [MeV]
q=3b
q=−4b
92Ni
11
12
13
14
15
R [fm]

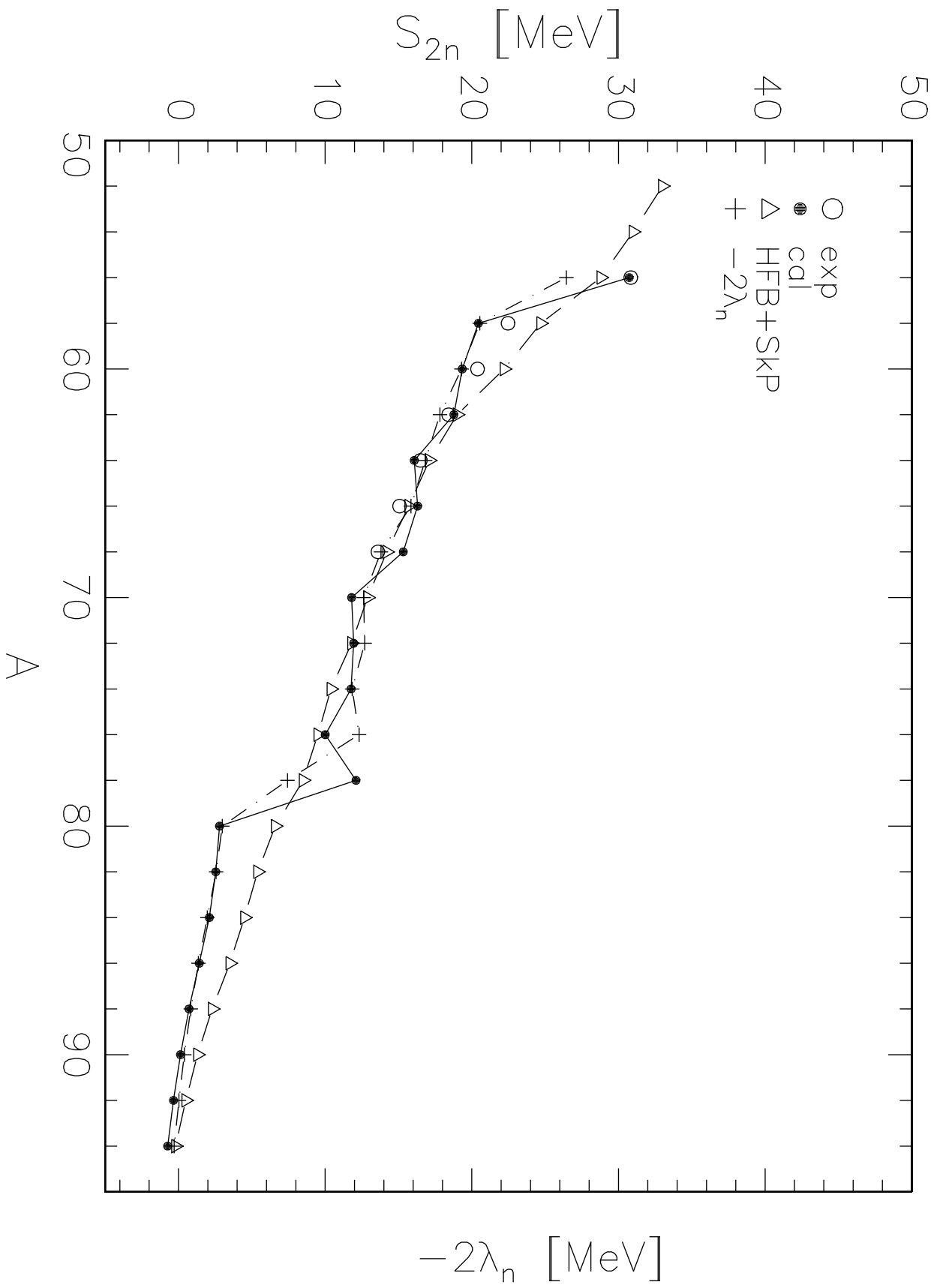
S_{2n} [MeV]
0
10
20
30
40
50
A
50
60
70
80
90
$-2\lambda_n$ [MeV]
O exp
● cal
△ HFB+SkP
+ $-2\lambda_n$